EUROFUSION WPMAG-PR(15) 14302

L. Savoldi et al.

Analyses of low- and high-margin Quench Propagation in the European DEMO TF Coil Winding Pack

Preprint of Paper to be submitted for publication in
IEEE Transactions on Plasma Science

This work has been carried out within the framework of the EUROfusion Consortium and has received funding from the Euratom research and training programme 2014-2018 under grant agreement No 633053. The views and opinions expressed herein do not necessarily reflect those of the European Commission.

Quench Propagation in the European DEMO TF Coil Winding Pack: a First Analysis with the 4C Code

Laura Savoldi, Roberto Bonifetto, Roberto Zanino
NEMO group, Dipartimento Energia,
Politecnico di Torino, Torino, Italy
roberto.zanino@polito.it

Luigi Muzzi
ENEA
Frascati, Italy

***Abstract*—Superconducting Toroidal Field (TF) coils composed of a winding pack (WP) without radial plates, encapsulated in a steel casing, are currently being studied in the framework of the EUROfusion Work Package Magnets (WPMAG). The ENEA 2014 TF WP design consists of graded (Nb3Sn + NbTi), double-layer wound rectangular cable-in-conduit conductors, for which operational as well as accidental transients must be carefully investigated. The paper presents the analysis of the quench propagation inside the TF WP proposed in 2014 by ENEA using the state-of-the-art thermal-hydraulic code 4C. Different locations are considered for the quench initiation and namely: 1) at the maximum temperature margin ΔT_{mar}^{max}, resulting in the most severe hot spot condition and 2) at the minimum temperature margin ΔT_{mar}^{min}, to analyze the most probable event. The evolution of voltage, normal zone, hot spot temperature and maximum pressure in the TF WP is computed comparing the results from the two cases, highlighting the role of heat diffusion inside the TF WP.**

Keywords— DEMO, superconducting magnets, quench, thermal-hydraulic analysis

I. Introduction

A "roadmap to fusion electricity by 2050" has been recently proposed and approved by the European Commission [1], which foresees the design of an European DEMO reactor, see Fig. 1, as the step following ITER, aimed at the demonstration of the feasibility of the production of electricity from fusion energy.

According to the current design, the DEMO toroidal field (TF) magnets should be composed by a compact winding pack (WP) without radial plates, encapsulated in a steel casing [3], see Fig. 2. The TF WP design proposed by ENEA in 2014 consists of graded (Nb3Sn + NbTi), double-layer wound rectangular cable-in-conduit conductors (CICC) [4], [5], see Fig. 3, to be cooled layer-by-layer with Supercritical Helium (SHe) at 4.5 K and 0.6 MPa. Such a big difference with respect to the ITER (pancake wound) TF magnets requires a new detailed analysis of operational and accidental transients, to be performed with reliable numerical tools, such as the 4C code [6].

4C, developed in the past years at Politecnico di Torino, is the state-of-the-art tool for the thermal-hydraulic analysis of SC magnet systems for fusion applications; it was validated against experimental results for different types of transients [7], [8], [9], [10] and also already applied to the investigation of the quench propagation in an ITER TF magnet [11]. After a benchmark with THEA code performed for the purpose of this study within the WPMAG project, the 4C code is applied here to the analysis of the quench propagation inside the DEMO TF WP proposed in 2014 by ENEA, assuming the quench initiation occurs at either of two different locations in the TF WP [12], and namely at the maximum or at the minimum temperature margin ΔT_{mar}. This choice follows the rationale that the quench propagating from the location at the maximum ΔT_{mar} will develop and travel very slowly, inducing the highest hot spot temperature in the conductor, while on the other hand the quench is most likely to initiate at minimum ΔT_{mar}. Relying on the 4C model of the TF conductor and TF WP already presented in [13], here we present first the setup for the quench simulations, and then we discuss the computed results. Due to the importance of the thermal insulation between turns and layers in the TF WP, discussed in the paper, it is worth to recall the thickness of the different insulation layers as described in [4] and reported in [13]:

- tape insulation of 1 mm around each conductor turn;
- additional insulation layer of 2 mm between the 2 layers inside each double-layer (DL);
- insulation layer of 1 mm surrounding each DL.

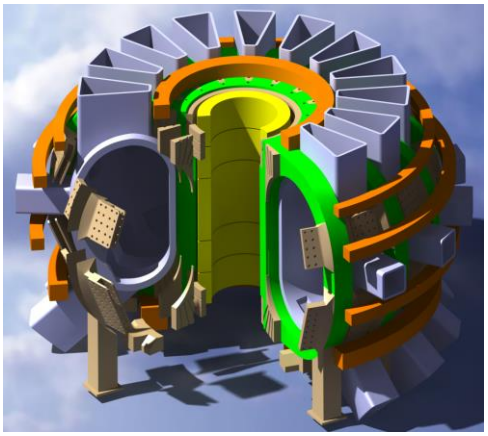

Fig. 1. Sketch of the European DEMO reactor. [2]

Work partially funded by EUROfusion.

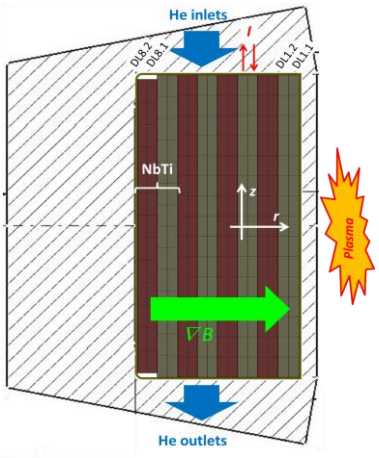

Fig. 2. Schematic view of the ENEA 2014 WP design for the EU DEMO. The two channels in the x-th double layer (DL) are named DLx.1 or 2.

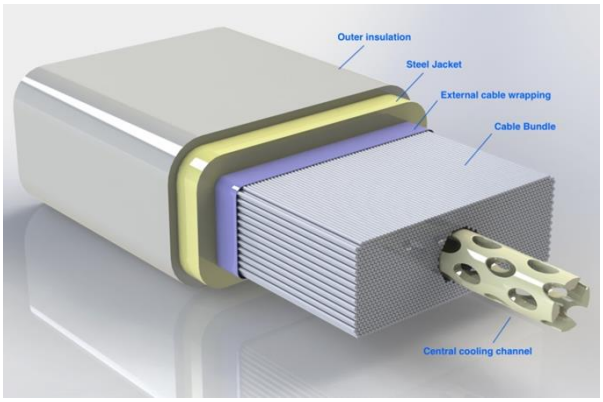

Fig. 3. ENEA CICC for the innermost layer of the EU DEMO TF WP [4].

II. Quench Simulation Setup

A. Localizing the quench initiation

The magnetic field in a cross section of the TF WP during a plasma pulse is reported in [13] according to [14], showing a minimum in the outermost Nb_3Sn layer DL 6.2 and the maximum in the innermost layer.

In order to compute the distribution of the temperature margin during a plasma pulse, we consider that 6 g/s of fresh SHe at 4.5 K and 0.6 MPa are provided to each hydraulic channel (8 g/s in the case of NbTi layers). The boundary conditions are kept constant during the entire transients since no circuit model is included in the simulations at this time. The temperature distribution computed by the 4C code inside the entire TF WP is shown in Fig. 4a, where the effect of the top side inlet is clearly visible, while the map of the temperature margin ΔT_{mar} is reported in Fig. 4b. The minimum ΔT_{mar} (~0.7 K) is located as expected in the inner layers, i.e. DL 2.1 in this case, due to the conductor grading (DL 1 is designed to have a ΔT_{mar} ~0.5 K higher than DL 2, without nuclear heating) and to the heat conduction from the innermost (most loaded) DL 1 to the neighboring DL 2, while the maximum ΔT_{mar} (~9.4 K) corresponds to the outermost Nb_3Sn layer DL 6.2. As a consequence, in our simulations we will consider the following two cases

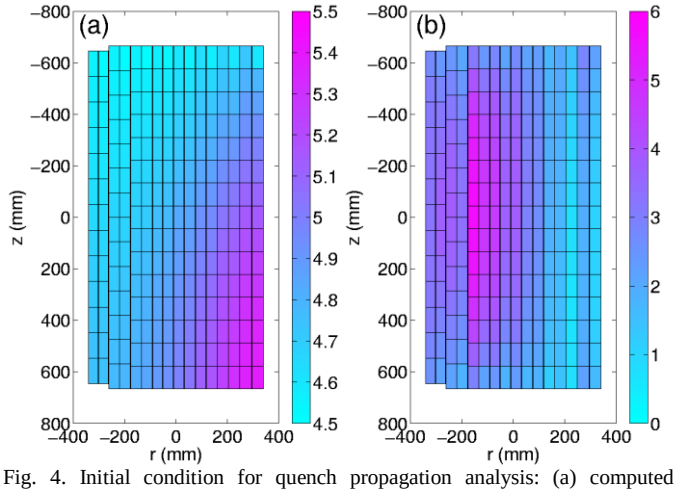

Fig. 4. Initial condition for quench propagation analysis: (a) computed temperature distribution (K) and (b) computed ΔT_{mar} distribution (K) in the WP at the ΔT_{mar}^{max} poloidal location.

- Case A = quench initiated at ΔT_{mar}^{max} (DL 6.2) and
- Case B = quench initiated at ΔT_{mar}^{min} (DL 2.1).

B. Current and heat load scenario

In the simulations, a quench initiated at full operating current (I = 81.7 kA) during the plasma pulse is considered. After quench detection and a reasonable time delay, see below for details, the current is then dumped with an exponential decay, with time constant of 23 s (note that the corresponding AC losses are not considered in the present study). A uniform nuclear heat load on each single layer is considered [15], as reported in [13]. To initiate the quench, a localized heating (54 kW/m in Case A and 8 kW/m in Case B, i.e. ~2×MQE as agreed in [12]) is applied for 100 ms in the simulations, on a length of 1 m around the two locations highlighted above. After 100 ms also the nuclear heating is conservatively switched off.

C. Quench detection

The quench detection threshold in the simulations has been set at 0.5 V, with a delay τ_{del} = 2 s before the current dump. The analysis is carried out for a total duration of 100 s.

D. Numerics

Finite elements are adopted for the solution of the problem, with an upwind scheme for the solution of the equations involving the flow variables. The solution is computed with a fully implicit time scheme on each hydraulic channel separately. The coupling between neighboring turns of the same layer is also evaluated in implicit, while the coupling between neighboring layers, modeled here in the same way as described in [13], is performed explicitly in time [16] in view of the much slower time scale of the transverse diffusion between neighboring conductors with respect to the time scales of the longitudinal heat transfer. The time-step is automatically adapted by the code between a minimum value (Δt_{min} = 1 ms) and a maximum value (Δt_{max} = 200 ms). Also the spatial mesh is adapted, following the propagation of the quench front. All these numerical parameters are the results of an accurate convergence analysis.

III. Discussion of the Computed Results

A selection of the computed results is shown in Figs. 5-8. In Fig. 5 the computed voltage evolution in the DL where the quench is initiated, as well as in the neighboring ones, is reported for both cases, together with the current evolution. In Case A, the voltage evolution during the quench initiation phase is much slower than in Case B, and it takes ~20 s to reach the quench detection threshold (to be compared to ~2 s in Case B).

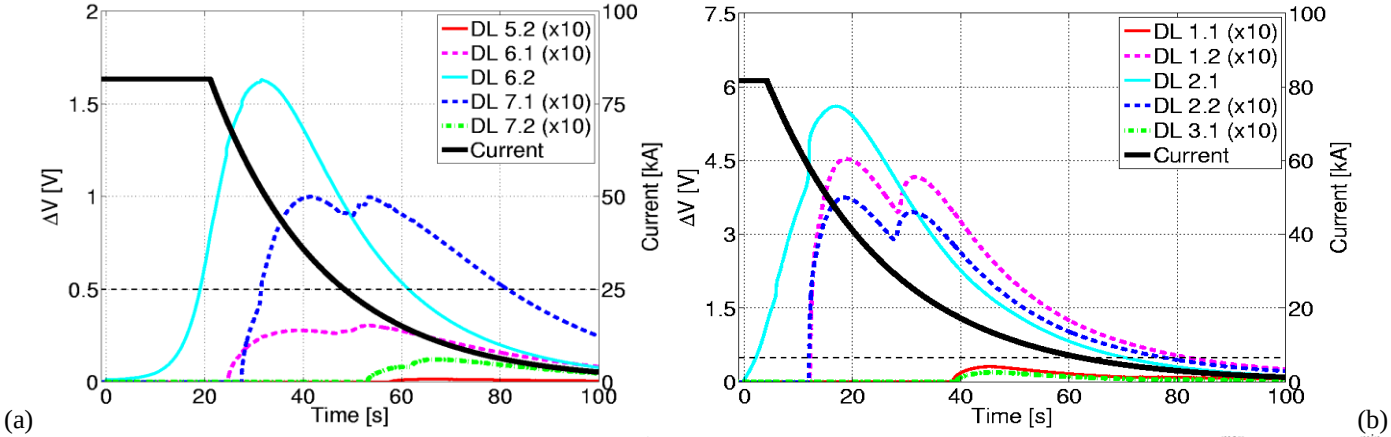

Fig. 5. Computed voltage evolution in the DLs involved by the quench (left axis) and current evolution (right axis) during the quench at ΔT_{mar}^{max} (a) and ΔT_{mar}^{min} (b), respectively. The black dashed thin line shows the quench detection threshold (0.5 V).

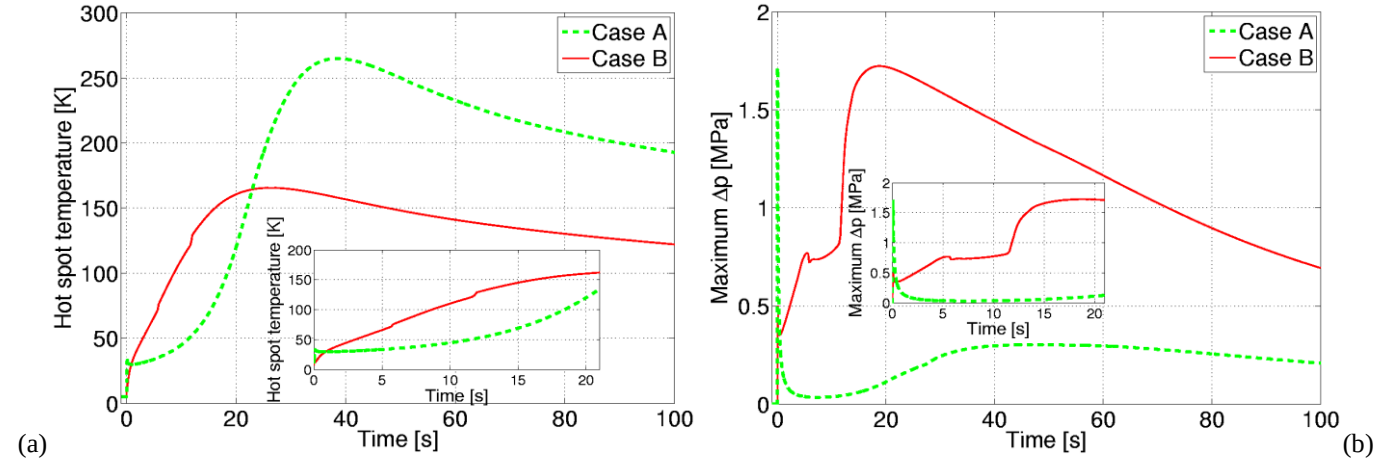

Fig. 6. Computed hot-spot temperature evolution (a) and maximum pressurization (b), in DL 6.2 (Case A) and DL 2.1 (Case B), respectively, during the quench. The first phases (before the dump) are reported in the insets.

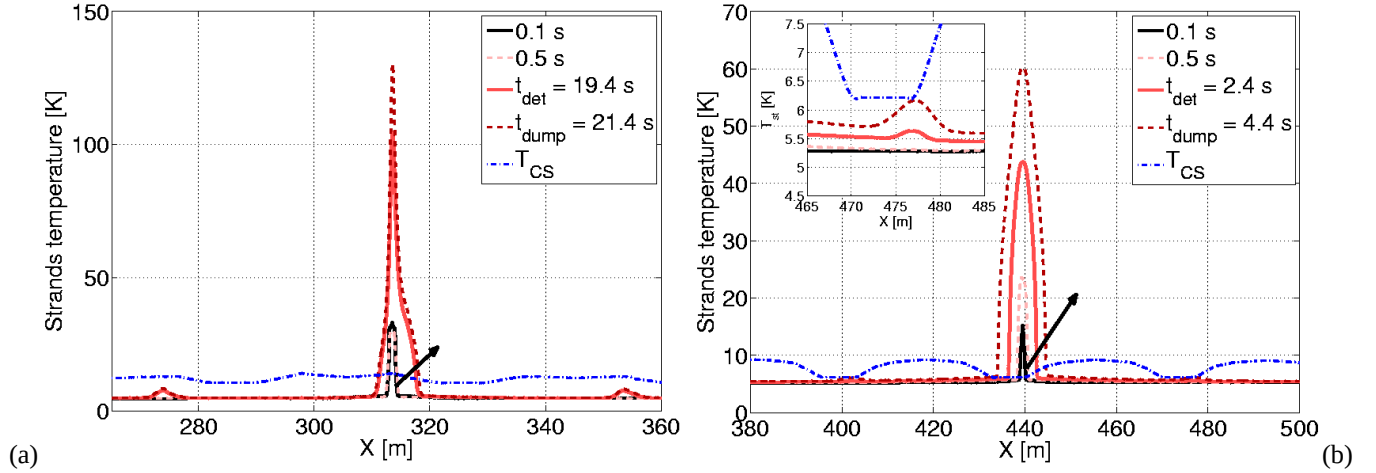

Fig. 7. Map of the computed temperature distribution in the strands along DL 6.2 for Case A (a) and DL 2.1 for Case B (b), at selected times of the transient (t_{det} corresponds to the time at which the quench is detected). The T_{CS} distribution is also reported (blue dash-dotted line).

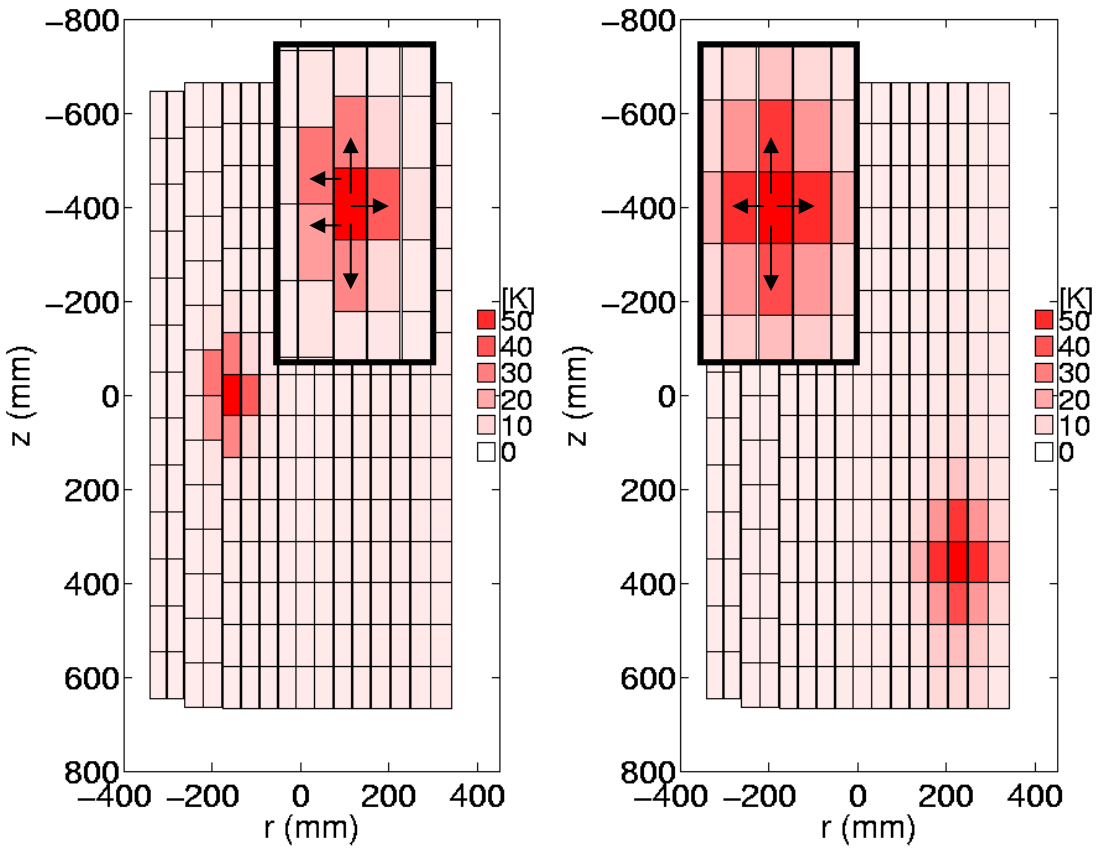

Fig. 8. Map of the computed temperature distribution in the TF WP cross section at the time and location of the maximum hot spot temperature in Case A (a) and Case B (b), respectively. (All temperatures above 50 K are represented as equal to 50 K in the figure.)

In the time up to the dump, the hot spot temperature increases up to ~130 K and 60 K respectively in Case A and Case B, see Fig. 6a and Fig. 7. When the current is dumped, the hot spot continues to increase in both cases reaching a peak value of ~260 K and 160 K, respectively. Note, however, that these values do *not* account for any AC losses during the current dump, which would lead to a further increase of the temperature. On the other hand, the hot spot temperature can be partly influenced by the introduction of 2×MQE to initiate the quench [12]. This, especially in Case A, leads to the use of a quite high input power (54 kW/m), which is indeed difficult to be reached during real magnet operation.

The peak pressurization reaches ~1.7 MPa in Case A during the heating phase that initiates the quench, see Fig. 6b – such a high value is however driven by the external heating more than by the joule heating. In Case B a similar peak value is reached but during the dump phase, see Fig. 6b, when the pressure rise in Case A is only of ~0.3 MPa.

Figure 7 shows the strands temperature profiles along the layer where the quench is initiated, for both Case A and Case B, up to the current dump, together with T_{CS}. It is shown that in Case A the quench propagates by advection upstream and downstream along the turn where the initiation region is located in view of the high margin along the conductor, while in Case B the quench is almost to be initiated also in neighboring turns of the same conductor right before the current dump (see inset Fig. 7b). Note, however, that the values computed before the current dump could be overestimated, both in terms of temperature and pressure increase, in view of the absence of even a simplified model of the cooling circuit for the TF WP.

On a longer timescale, the heat conduction through the jacket drives the heat transfer to the *adjacent turns*, where the quench is also initiated, see the vertical arrows in Fig. 8, where the temperature maps on the TF WP cross section, computed for both cases at the time when the hot spot temperature is reached, are reported. From Fig. 7 it can be checked that by that time the quench has not propagated by advection to the neighboring turns yet, confirming that the heat propagation visible in Fig. 8 occurs only by thermal conduction. For the same heat transfer mechanism, although the quench is initiated in a single DL, the neighboring DLs are also progressively affected, see the horizontal arrows in Fig. 8, as well as the voltage increase in the DL 6.1 and 7.1 for Case A (Fig. 5a) and in DL 1.2 and 2.2 for Case B (Fig. 5b), respectively.

IV. Remarks on the Thermal Coupling Inside the TF WP

The relevance of including the inter-turn and inter-layer thermal coupling, a feature peculiar of the 4C code, is further emphasized in Fig. 9, where the comparison with the computed results in the case of adiabatic conductors is reported.

As a first main difference, with respect to the case where transverse heat transfer in the TF WP is duly accounted for, the

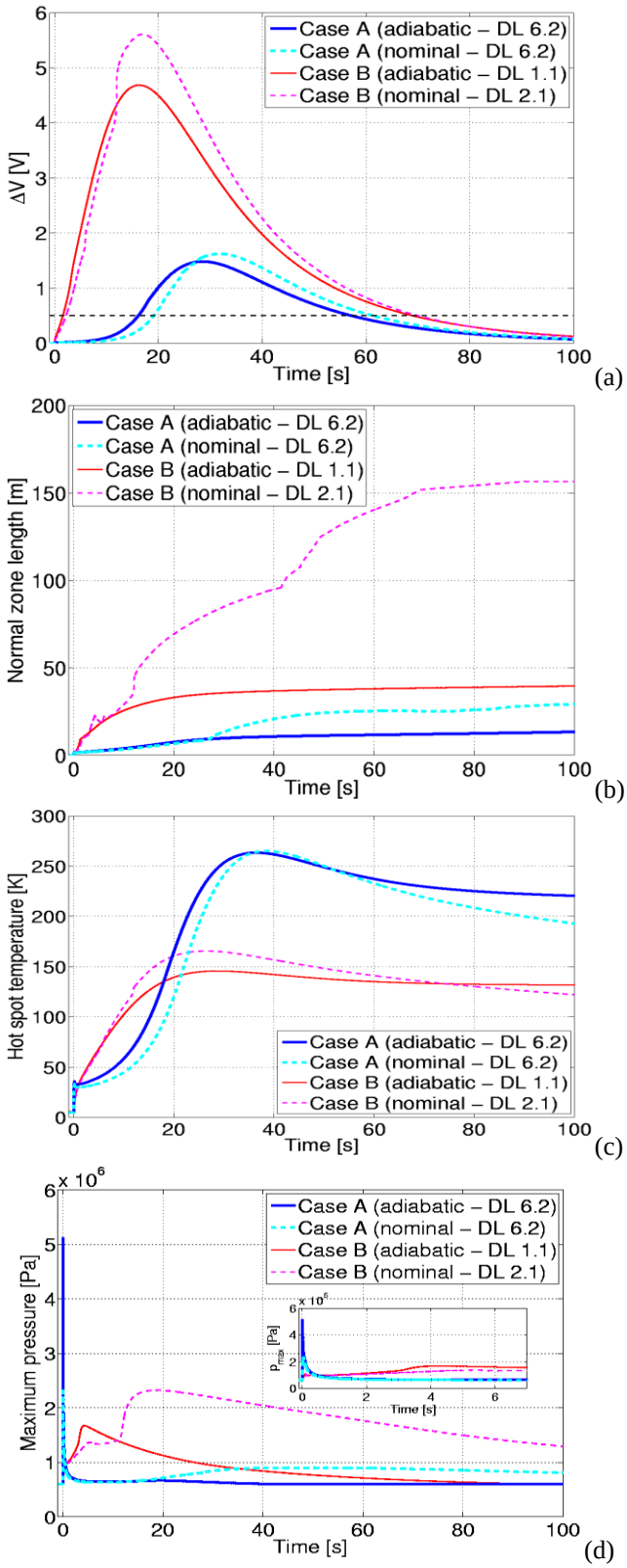

Fig. 9. Comparison between simulation with nominal thermal coupling between neighboring conductors (dashed lines) and adiabatic conductors (solid lines) for both Case A and Case B: (a) Total voltage and (b) normal zone length (c) hot spot and (d) maximum pressure in the quenched DL, respectively.

most critical DL, i.e. the DL where the minimum ΔT_{mar} is

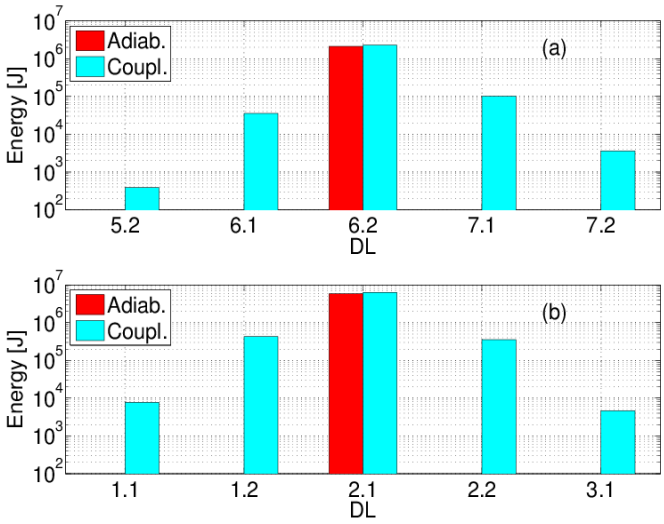

Fig. 10. Computed energy released up to 150 s in the quenched DLs in adiabatic and non–adiabatic simulations, for Case A (a) and Case B (b), respectively.

located, becomes DL 1.1 (in view of the higher nuclear load than DL 2.1, which cannot be transferred to the cooler neighboring layers), so that in the adiabatic condition the quench analysis is carried out for Case B in this conductor.

In Fig. 9a the voltage evolution is reported, showing that initially a beneficial effect of the thermal coupling reduces the total voltage with respect to the adiabatic case. However, on longer time scales, the adiabatic simulation is not able to capture the voltage increase due to the quenching of the neighboring turns, which needs the transverse thermal conduction in the winding pack to be triggered, see also the computed normal zone evolution in Fig. 9b. While the hot spot temperature is not significantly affected by the heat transfer across the TF WP, see Fig. 9c, as expected from the fact that the quench initiation is very similar, see Fig. 9a, the pressure peak during the current dump phase is much lower if the quench propagation to the neighboring turns is not accounted for, see Fig. 9d.

A clear picture of the role of the thermal diffusion across the winding pack is given in Fig. 10, where the deposited energy in all the quenched DLs is reported. In Case A the energy deposited in the DL 6.2, evaluated at 150 s from the starting of the heating, is 2.3 MJ and the energy deposited in the neighboring DLs is 0.14 MJ, contributing up to the ~6% of the total energy; in Case B, instead, neglecting the inter-turn/inter-layer thermal coupling the energy deposited in the DL 2.1 is 5.8 MJ, while the total energy deposited in all DLs (2.1 and the neighboring ones) in the nominal simulation is 7.2 MJ: the adiabatic simulation underestimates the deposited energy by ~19%.

V. Conclusions

The first analysis of quench propagation in a European DEMO TF winding pack has been performed with the 4C code.

The ENEA 2014 design has been considered and the results have been presented for both cases of quench initiation

at the minimum and at the maximum $\Delta T_{mar.}$ From the quantitative point of view, with the quench detection system parameters adopted here and neglecting the AC loss generation during the dump, the simulation gives $T_{hot\ spot} >$ 260 K in the most critical case and a pressure rise up to ~1.7 MPa during the current dump. The latter can be captured only if the heat diffusion to the neighboring turns of the quenched layer is properly accounted for. From the simulated results, a quench is also induced in the neighboring layers by heat diffusion through conductor jacket and insulation in both cases analyzed here.

In perspective, we plan to refine the simulation, including a rough model of the TF WP cooling circuit, to provide the simulation with a set of self-consistent boundary conditions [17], as well as to develop a model of the casing, thermally coupled to the TF WP, and of its cooling loop, to compute a more realistic temperature distribution in the TF WP during plasma pulses.

ACKNOWLEDGMENT

This work has been carried out within the framework of the EUROfusion Consortium and has received funding from the Euratom research and training programme 2014-2018 under grant agreement No 633053. The views and opinions expressed herein do not necessarily reflect those of the European Commission.

REFERENCES

[1] F. Romanelli, et al., "Fusion electricity. A roadmap to the realisation of fusion energy", https://www.euro-fusion.org/wpcms/wp-content/uploads/2013/01/JG12.356-web.pdf

[2] S. Turtù, A. Anemona, M. E. Biancolini, and C. Brutti, "Electromagnetic and Mechanical Analysis of candidate prototype LTS conductors, winding pack and TF coil casing", EFDA_D_2LNP3B v2.0, 22/12/2013.

[3] EFDA PPPT, "DEMO geometry derivation from PROCESS code based on the current knowledge", EFDA_D_2LFUG2, 30/04/2014.

[4] L. Muzzi, "Design of TF Winding Pack Option 2 (WP#2) and of "ENEA" LTS cable", EFDA_D_2HEYFG, 23/01/2015.

[5] P. Bruzzone, K. Sedlak, D. Uglietti, N. Bykovsky, L. Muzzi, G. De Marzi, G. Celentano, A. della Corte, S. Turtù, and M. Seri, "LTS and HTS High Current Conductor Development for DEMO", submitted to Fus. Eng. Des., 2015.

[6] L. Savoldi Richard, F. Casella, B. Fiori, and R. Zanino, "The 4C Code for the Cryogenic Circuit Conductor and Coil modeling in ITER", Cryogenics, vol. 50, pp. 167–176, 2010.

[7] R. Zanino, R. Bonifetto, R. Heller, and L. Savoldi Richard, "Validation of the 4C Thermal-Hydraulic Code against 25 kA Safety Discharge in the ITER Toroidal Field Model Coil (TFMC)", IEEE Trans. Appl. Supercond., vol. 21, pp. 1948–1962, 2011.

[8] R. Bonifetto, A. Kholia, B. Renard, K. Riβe, L. Savoldi Richard, and R. Zanino, "Modeling of W7-X superconducting coil cool-down using the 4C code", Fus. Eng. Des., vol. 86, pp. 1549–1552, 2011.

[9] R. Zanino, R. Bonifetto, F. Casella, and L. Savoldi Richard, "Validation of the 4C code against data from the HELIOS loop at CEA Grenoble", Cryogenics, vol. 53, pp. 25–30, 2013.

[10] R. Zanino, R. Bonifetto, C. Hoa, and L. Savoldi Richard, "Verification of the Predictive Capabilities of the 4C Code Cryogenic Circuit Model", AIP Conference Proceedings, vol. 1573, pp. 1586–1593, 2014.

[11] R. Zanino, D. Bessette, and L. Savoldi Richard, "Quench analysis of an ITER TF coil", Fus. Eng. Des., vol. 85, pp.752–760, 2010.

[12] R. Bonifetto, B. Lacroix, M. Lewandowska, L. Savoldi, K. Sedlak, R. Vallcorba, and R. Zanino, "Common approaches for quench analyses", EFDA_D_2M6DW4, 14/01/2015.

[13] R. Zanino, R. Bonifetto, L. Savoldi, and L. Muzzi, "4C Code Analysis of High-Margin Quench Propagation in a DEMO TF Coil", Proceedings of the Symposium on Fusion Engineering 2015, Austin, Texas, May 31 – June 4, 2015.

[14] A. Torre, Personal communication, 05/12/2014, unpublished.

[15] L. Zani, and U. Fischer, "Advanced definition of neutronic heat load density map on DEMO TF coils", EFDA_D_2MFVCA, 18/10/2014.

[16] L. Savoldi, and R. Zanino, "M&M: Multi-conductor Mithrandir code for the simulation of thermal-hydraulic transients in superconducting magnets", Cryogenics, vol. 40, pp. 179–189, 2000.

[17] L. Savoldi Richard, R. Zanino and L. Bottura, "Simulation of thermal-hydraulic tranisents in two-channel CICC with self-consistent boundary conditions", Adv, Cryo. Eng., vol 45, pp. 697-704, 2000.